Sub-Domain Decomposition Iterative Method Combined With ACA: An Efficient Technique for the Scattering From a Large Highly Conducting Rough Sea Surface

Christophe Bourlier, Sami Bellez, Hongkun Li, and Gildas Kubické

***Abstract*—The sub-domain decomposition iterative method (SDIM) is presented to solve efficiently a large linear system obtained by sampling the boundary integral equations from the method of moments. Then, this new technique is tested on the electromagnetic scattering problem from a large highly conducting one-dimensional rough sea surface. The diagonal blocks are the local impedance matrices corresponding to the geometry sub-domains while the off-diagonal blocks are the coupling matrices describing the interaction between two different sub-domains. The principle of SDIM is to invert the impedance matrix by blocks reducing significantly the complexity in comparison to a direct LU inversion of the whole impedance matrix. In addition, to accelerate the matrix-vector products and to reduce the memory requirement, the adaptive cross approximation (ACA) is applied to compress the sub-domain coupling matrices. For microwave frequencies, the results show that SDIM converges rapidly and faster for the TM polarization. Moreover, the mean compression ratio of ACA is of the order of 98%, which makes this method very efficient.**

***Index Terms*—Adaptive cross approximation, electromagnetic scattering by rough surfaces, iterative methods, method of moments (MoM).**

I. Introduction

THE study of the microwave scattering from rough sea surfaces is a subject of great interest. The applications of such research concern many areas such as remote sensing, radar surveillance, optics, and ocean acoustics.

The well-known Method of Moments (MoM) [1]–[3] is a way of solving rigorously the scattering problem by converting the boundary integral equation into a linear system, in which the impedance matrix must be inverted to determine the surface currents. This method has been widely used to calculate the scattering by perfectly conducting rough sea surfaces as well as by highly conducting rough sea surfaces by applying the impedance boundary condition (IBC). However, the direct solution of the linear system through LU decomposition is classically limited by a $\mathcal{O}(N^3)$ and $\mathcal{O}(N^2)$ complexities in CPU time and memory requirement, respectively, where N is the number of unknowns. This is computationally very expensive for electrically large rough surfaces and has lead to use iterative methods that significantly reduce the storage and computation cost.

Among these methods, the stationary iterative forward–backward method (FB) [4] combined with the spectral acceleration (SA) [5], is the most efficient one for the scattering from highly conducting rough sea surfaces. This method has also been successfully incorporated into the iterative schemes of propagation-inside-layer-expansion (PILE) and extended propagation-inside-layer-expansion (EPILE) solvers aimed to study the scattering from an object located below, on and above a rough sea surface, respectively [6]–[10].

For more than a decade, another family of fast direct solvers has been developed to deal with a very large number of unknowns. These methods are fundamentally based on the fact that the entire problem geometry can be subdivided into several overlapping or non-overlapping sub-domains (blocks) and the MoM impedance matrix can also be partitioned into local impedance sub-matrices. They represent the interaction between the basis functions within each block, while the coupling impedance sub-matrices describe the interaction between the basis functions of the blocks. The problem solution is then reduced to successively solve a set of impedance sub-matrix equations. PILE, EPILE, and characteristic basis function method (CBFM) [11] are based on this concept. The latter has been applied for the scattering from rough terrain profiles and in order to minimize the computational cost [12], [13], accelerations are integrated by using FB method, the physical optics approximation, etc.

In the same way, this paper presents the sub-domain decomposition iterative method (SDIM) to solve efficiently a large linear system obtained by sampling the integral equations through a MoM with pulse basis functions and point matching. Then, this new technique is tested on the microwave electromagnetic scattering problem from a large IBC rough one-dimensional sea surface. Its principle is to invert the impedance matrix by blocks, reducing significantly the complexity in comparison to a direct LU inversion of the whole impedance matrix. Furthermore, it is possible to exploit the

Manuscript received June 16, 2014; revised September 17, 2014; accepted October 30, 2014. Date of publication November 24, 2014; date of current version January 30, 2015.

C. Bourlier, S. Bellez, and H. Li are with the IETR (Institut d'Electronique et des Télécommunications de Rennes) Laboratory, LUNAM Université, Université de Nantes, La Chantrerie, 44306 Nantes, France.

G. Kubické is with the DGA/DT/MI (Direction Générale de l'Armement—Direction Technique—Maîtrise de l'Information), CGN1 Division, 35170 Bruz, France (e-mail: gildas.kubicke@intradef.gouv.fr).

Color versions of one or more of the figures in this paper are available online at http://ieeexplore.ieee.org.

Digital Object Identifier 10.1109/TAP.2014.2373395

0018-926X © 2014 IEEE. Personal use is permitted, but republication/redistribution requires IEEE permission.
See http://www.ieee.org/publications_standards/publications/rights/index.html for more information.

low-rank properties of the coupling impedance sub-matrices for the purpose to perform fast matrix-vector products. One of the most relevant algorithms carrying out this task is the adaptive cross approximation (ACA), which expresses any matrix as a product of two compressed matrices. This algebraic method, developed in 2000 by Bebendorf [14], [15], was then applied to electromagnetics [16]–[20] and can be seen as a truncated and partially pivoted Gaussian elimination [14].

Then, SDIM is hybridized with ACA technique to accelerate the matrix-vector products and to decrease the memory requirement. In addition, to reduce the complexity of SDIM, the approximation based on the fact that the electromagnetic interaction between far blocks is weak, is tested.

This paper is organized as follows. Section II presents the mathematical formulation of SDIM, its complexity and its resulting complexity when ACA is applied. Section III presents numerical results and the last section gives concluding remarks.

II. Theory

A. Mathematical Formulation of SDIM

The MoM [1] for the electromagnetic scattering problem results in a set of linear system of algebraic equations that are cast in matrix form as follows:

$$\bar{\boldsymbol{Z}}\boldsymbol{X} = \boldsymbol{b} \tag{1}$$

where $\bar{\boldsymbol{Z}}$ is the known MoM impedance matrix of sizes $N \times N$, $\boldsymbol{b}$ is an $N \times 1$ known excitation vector, and $\boldsymbol{X}$, is the unknown solution vector of sizes $N \times 1$, with N the number of unknowns needed to accurately describe the current distribution on the surface. For electrically large geometries, N becomes prohibitively large, and this rules out the option of direct matrix inversion for computing the vector $\boldsymbol{X}$.

To overcome this issue, the SDIM is developed. It consists in splitting the surface S into P sub-domains $S_i (S = S_1 \cup S_2 \cup \cdots \cup S_P)$. Then, it first computes the current density on each isolated sub-surface $S_i(\boldsymbol{X}_i)$ and next, from an iterative scheme, it updates the current density by interacting the sub-domains between them.

The matrix $\bar{\boldsymbol{Z}}$ can be partitioned as

$$\bar{\boldsymbol{Z}} = \begin{bmatrix} \bar{\boldsymbol{Z}}_{1,1} & \bar{\boldsymbol{Z}}_{2,1} & \dots & \bar{\boldsymbol{Z}}_{P,1} \\ \bar{\boldsymbol{Z}}_{1,2} & \bar{\boldsymbol{Z}}_{2,2} & \dots & \bar{\boldsymbol{Z}}_{P,2} \\ \vdots & \vdots & \ddots & \vdots \\ \bar{\boldsymbol{Z}}_{1,P} & \bar{\boldsymbol{Z}}_{2,P} & \dots & \bar{\boldsymbol{Z}}_{P,P} \end{bmatrix} \tag{2}$$

where P^2 is the number of sub-matrices $\bar{\boldsymbol{Z}}_{i,p}$ of sizes $N_i \times N_p$ and $N = \sum_{i=1}^{P} N_i$.

The matrix $\bar{\boldsymbol{A}}$ is decomposed as follows:

$$\bar{\boldsymbol{Z}} = \bar{\boldsymbol{A}} + \bar{\boldsymbol{C}} \tag{3}$$

where

$$\bar{\boldsymbol{A}} = \begin{bmatrix} \bar{\boldsymbol{Z}}_{1,1} & \bar{\boldsymbol{0}} & \dots & \bar{\boldsymbol{0}} \\ \bar{\boldsymbol{0}} & \bar{\boldsymbol{Z}}_{2,2} & \dots & \bar{\boldsymbol{0}} \\ \vdots & \vdots & \ddots & \vdots \\ \bar{\boldsymbol{0}} & \bar{\boldsymbol{0}} & \dots & \bar{\boldsymbol{Z}}_{P,P} \end{bmatrix} \tag{4}$$

and

$$\bar{\boldsymbol{C}} = \begin{bmatrix} \bar{\boldsymbol{0}} & \bar{\boldsymbol{Z}}_{2,1} & \dots & \bar{\boldsymbol{Z}}_{P,1} \\ \bar{\boldsymbol{Z}}_{1,2} & \bar{\boldsymbol{0}} & \dots & \bar{\boldsymbol{Z}}_{P,2} \\ \vdots & \vdots & \ddots & \vdots \\ \bar{\boldsymbol{Z}}_{1,P} & \bar{\boldsymbol{Z}}_{2,P} & \dots & \bar{\boldsymbol{0}} \end{bmatrix}. \tag{5}$$

The matrix $\bar{\boldsymbol{A}}$ is a matrix of sizes $N \times N$ which contains the diagonal blocks $\bar{\boldsymbol{Z}}_{p,p} (i = p \in [1; P])$ and $\bar{\boldsymbol{C}}$ a matrix of sizes $N \times N$ which contains the off-diagonal blocks $\bar{\boldsymbol{Z}}_{i,p} (i \neq p)$. It corresponds to the coupling matrix between the blocks.

The matrix $\bar{\boldsymbol{C}}$ is decomposed as follows $\bar{\boldsymbol{C}} = \bar{\boldsymbol{U}}\bar{\boldsymbol{B}}\bar{\boldsymbol{V}}$, where $\bar{\boldsymbol{U}}$ is a lower triangular matrix, $\bar{\boldsymbol{B}}$ a diagonal matrix and $\bar{\boldsymbol{V}}$ an upper triangular matrix. These three matrices are of sizes $N \times N$. Then, from [21, (Eq. (3.54))], we have

$$\begin{aligned} \bar{\boldsymbol{Z}}^{-1} &= \left(\bar{\boldsymbol{A}} + \bar{\boldsymbol{U}}\bar{\boldsymbol{B}}\bar{\boldsymbol{V}}\right)^{-1} \\ &= \bar{\boldsymbol{A}}^{-1} - \bar{\boldsymbol{A}}^{-1}\bar{\boldsymbol{U}}\left(\bar{\boldsymbol{I}} + \bar{\boldsymbol{B}}\bar{\boldsymbol{V}}\bar{\boldsymbol{A}}^{-1}\bar{\boldsymbol{U}}\right)^{-1}\bar{\boldsymbol{B}}\bar{\boldsymbol{V}}\bar{\boldsymbol{A}}^{-1} \end{aligned} \tag{6}$$

where the matrices $\bar{\boldsymbol{A}}$ and $\bar{\boldsymbol{I}} + \bar{\boldsymbol{B}}\bar{\boldsymbol{V}}\bar{\boldsymbol{A}}^{-1}\bar{\boldsymbol{U}}$ are assumed to be invertible and $\bar{\boldsymbol{I}}$ stands for the identity matrix.

For any matrix $\bar{\boldsymbol{T}}$, the following Taylor series expansion $1/(1+\bar{\boldsymbol{T}}) = \sum_{k=0}^{\infty}(-1)^k\bar{\boldsymbol{T}}^k$ can be applied if the spectral radius (modulus of its eigenvalue, which has the highest modulus) of $\bar{\boldsymbol{T}}$ is strictly smaller than one. Assuming that the spectral radius of the matrix $\bar{\boldsymbol{M}} = \bar{\boldsymbol{B}}\bar{\boldsymbol{V}}\bar{\boldsymbol{A}}^{-1}\bar{\boldsymbol{U}}$ is strictly smaller than one, then the use of the Taylor series expansion leads to

$$\begin{aligned} \bar{\boldsymbol{Z}}^{-1} &= \bar{\boldsymbol{A}}^{-1} - \bar{\boldsymbol{A}}^{-1}\bar{\boldsymbol{U}}\left[\sum_{k=0}^{k=\infty}(-1)^k\left(\bar{\boldsymbol{B}}\bar{\boldsymbol{V}}\bar{\boldsymbol{A}}^{-1}\bar{\boldsymbol{U}}\right)^k\right]\bar{\boldsymbol{B}}\bar{\boldsymbol{V}}\bar{\boldsymbol{A}}^{-1}. \\ &= \bar{\boldsymbol{A}}^{-1} - \bar{\boldsymbol{M}}_c\bar{\boldsymbol{A}}^{-1} + \bar{\boldsymbol{M}}_c^2\bar{\boldsymbol{A}}^{-1} - \bar{\boldsymbol{M}}_c^3\bar{\boldsymbol{A}}^{-1} + \cdots \\ &= \sum_{k=0}^{k=\infty}(-1)^k\bar{\boldsymbol{M}}_c^k\bar{\boldsymbol{A}}^{-1} \end{aligned} \tag{7}$$

where $\bar{\boldsymbol{M}}_c = \bar{\boldsymbol{A}}^{-1}\bar{\boldsymbol{C}}$ is the characteristic matrix of the sub-domains decomposition. From (7), The matrix-vector product $\boldsymbol{X} = \bar{\boldsymbol{Z}}^{-1}\boldsymbol{b} = \sum_{k=0}^{\infty}\boldsymbol{Y}^{(k)}$ can be written as

$$\begin{cases} \boldsymbol{Y}^{(0)} = \bar{\boldsymbol{A}}^{-1}\boldsymbol{b} \\ \boldsymbol{Y}^{(k)} = -\bar{\boldsymbol{M}}_c\boldsymbol{Y}^{(k-1)} \quad k > 0 \end{cases}. \tag{8}$$

From (4), the computation of $\bar{\boldsymbol{A}}^{-1}$ is straightforward, leading to

$$\bar{\boldsymbol{A}}^{-1} = \begin{bmatrix} \bar{\boldsymbol{Z}}_{1,1}^{-1} & \bar{\boldsymbol{0}} & \dots & \bar{\boldsymbol{0}} \\ \bar{\boldsymbol{0}} & \bar{\boldsymbol{Z}}_{2,2}^{-1} & \dots & \bar{\boldsymbol{0}} \\ \vdots & \vdots & \ddots & \vdots \\ \bar{\boldsymbol{0}} & \bar{\boldsymbol{0}} & \dots & \bar{\boldsymbol{Z}}_{P,P}^{-1} \end{bmatrix}. \tag{9}$$

Then, the matrix product $\bar{\boldsymbol{M}}_c = \bar{\boldsymbol{A}}^{-1}\bar{\boldsymbol{C}}$ leads to

$$\bar{\boldsymbol{M}}_c = \begin{bmatrix} \bar{\boldsymbol{0}} & \bar{\boldsymbol{Z}}_{1,1}^{-1}\bar{\boldsymbol{Z}}_{2,1} & \dots & \bar{\boldsymbol{Z}}_{1,1}^{-1}\bar{\boldsymbol{Z}}_{P,1} \\ \bar{\boldsymbol{Z}}_{2,2}^{-1}\bar{\boldsymbol{Z}}_{1,2} & \bar{\boldsymbol{0}} & \dots & \bar{\boldsymbol{Z}}_{2,2}^{-1}\bar{\boldsymbol{Z}}_{P,2} \\ \vdots & \vdots & \ddots & \vdots \\ \bar{\boldsymbol{Z}}_{P,P}^{-1}\bar{\boldsymbol{Z}}_{1,P} & \bar{\boldsymbol{Z}}_{P,P}^{-1}\bar{\boldsymbol{Z}}_{2,P} & \dots & \bar{\boldsymbol{0}} \end{bmatrix}. \tag{10}$$

Setting

$$\boldsymbol{Y}^{(k)} = \begin{bmatrix} \boldsymbol{Y}_1^{(k)} \\ \boldsymbol{Y}_2^{(k)} \\ \vdots \\ \boldsymbol{Y}_P^{(k)} \end{bmatrix}, \ \boldsymbol{b} = \begin{bmatrix} \boldsymbol{b}_1 \\ \boldsymbol{b}_2 \\ \vdots \\ \boldsymbol{b}_P \end{bmatrix} \tag{11}$$

from (8) and (10), one shows

$$\begin{cases} \boldsymbol{Y}_i^{(0)} = \bar{\boldsymbol{Z}}_{i,i}^{-1} \boldsymbol{b}_i \\ \boldsymbol{Y}_i^{(k)} = -\bar{\boldsymbol{Z}}_{i,i}^{-1} \sum_{p=1, p\neq i}^{P} \bar{\boldsymbol{Z}}_{p,i} \boldsymbol{Y}_p^{(k-1)} \ k > 0 \end{cases} \tag{12}$$

and the unknown vector $\boldsymbol{X}$ can be expressed as

$$\mathbf{X}^{(K_{\mathrm{SDIM}})} \approx \sum_{k=0}^{k=K_{\mathrm{SDIM}}} \mathbf{Y}^{(k)}. \tag{13}$$

The vectors $\{\boldsymbol{Y}_i^{(k)}\}$ and $\{\boldsymbol{b}_i\}(i \in [1; P])$ are of sizes $N_i \times 1$.

The convergence order K_{SDIM} is obtained from a criterion. For instance, it can be obtained when $\mathrm{norm}(\boldsymbol{X}^{(k+1)} - \boldsymbol{X}^{(k)})/\mathrm{norm}(\boldsymbol{X}^{(k)}) \leq \epsilon_0$, where ϵ_0 is a threshold and norm stands for the norm two.

It is interesting to note that the calculations of $\boldsymbol{Y}_i^{(0)}$ and $\boldsymbol{Y}_i^{(1)}$ are similar as to those of the characteristic basis function method (CBFM) [11]. Indeed, $\boldsymbol{Y}_i^{(0)}$ equals the primary basis function (PBF), whereas $-\bar{\boldsymbol{Z}}_{p,i}\boldsymbol{Y}_p^{(0)}$ gives the secondary basis functions (SBF). Next, the method differs from ours since a modified Gram–Schmidt process to construct ortho-normalized functions is applied to determine the unknown $\boldsymbol{X}$ with CBFM.

For $P = 2$ (two sub-domains), it can be shown that the SDIM algorithm is the same as EPILE one [3], [7] developed for the scattering from two illuminated scatterers. However, it would be different of the multi-levels EPILE method.

B. Complexity of SDIM

Let C_i be the complexity to invert $\bar{\boldsymbol{Z}}_{i,i}$ and $C_{p,i}$ the complexity for the matrix-vector product $\bar{\boldsymbol{Z}}_{p,i}\boldsymbol{Y}_p^{(k-1)}$. Then, the complexity of SDIM is

$$\begin{cases} \boldsymbol{Y}^{(0)} \rightarrow \sum_{i=1}^{P} \left[C_i + \mathcal{O}(N_i^2)\right] \\ \boldsymbol{Y}^{(k)} \rightarrow \sum_{i=1}^{P} \left[C_i + \mathcal{O}(N_i^2)\right] + \sum_{i=1}^{P} \sum_{p=1, p\neq i}^{P} C_{p,i} \end{cases} \tag{14}$$

where $\mathcal{O}(N_i^2)$ is the complexity of the matrix-vector product $\bar{\boldsymbol{Z}}_{i,i}^{-1}\boldsymbol{v}_i$. If $C_i = C_0$, $C_{p,i} = C_{0,0}$, and $N_i = N_0$ are constant, the resulting complexity to calculate $\boldsymbol{X}$ is then

$$C = P\Big\{C_0 + \mathcal{O}(N_0^2) + K_{\mathrm{SDIM}}\left[C_0 + \mathcal{O}(N_0^2) + (P-1)C_{0,0}\right]\Big\}. \tag{15}$$

If a direct LU inversion is applied to calculate $\bar{\boldsymbol{Z}}_{i,i}^{-1}$, then $C_0 = \mathcal{O}(N_0^3)$ and if the matrix $\bar{\boldsymbol{Z}}_{p,i}(p \neq i)$ is not compressed then $C_{0,0} = \mathcal{O}(N_0^2)$. Assuming that $P \ll N$, then

$$C \approx \mathcal{O}(N_0^3) P \left(1 + K_{\mathrm{SDIM}}\right). \tag{16}$$

Comparing with a direct LU inversion of the matrix $\bar{\boldsymbol{Z}}(\mathcal{O}(N^3)$ with $N = N_0 \times P)$, the SDIM is efficient if $(1 + K_{\mathrm{SDIM}}) \ll P^2$. Another advantage of SDIM is that the solution results from inversions and matrix-vector products of matrices of smaller sizes. Then, if N_0 is not too large, LU direct inversions can be applied to calculate $\{\bar{\boldsymbol{Z}}_{i,i}^{-1}\}$, which can not be possible from the whole matrix $\bar{\boldsymbol{Z}}$. In addition, the memory requirement becomes $\mathcal{O}(PN_0^2)$ instead of $\mathcal{O}(P^2N_0^2)$. Also, fast methods can be applied to calculate $\{\bar{\boldsymbol{Z}}_{i,i}^{-1}\boldsymbol{v}_i\}$, such as the forward–backward (FB) [4] method combined with the Spectral acceleration (SA) [5], which is very efficient for a sea surface [7]. In addition, if the coupling between the sub-domains is weak (far interactions), then the indexes p in (12) can be chosen as $p = \{i-1, i+1\}$ with $\max(p) = P$ and $\min(p) = 1$. Concerning the matrix-vector products, their complexity can be reduced by compressing the coupling sub-matrix $\bar{\boldsymbol{Z}}_{p,i}(p \neq i)$ from the ACA algorithm.

C. ACA Acceleration

The objective of the ACA algorithm is to approximate a given dense matrix $\bar{\boldsymbol{A}}$ of size $M \times N$ by an approximate matrix $\tilde{\boldsymbol{A}}$ (of size $M \times N$ too) obtained from a matrix product:

$$\tilde{\boldsymbol{A}} = \bar{\boldsymbol{U}}\bar{\boldsymbol{V}} \tag{17}$$

where $\bar{\boldsymbol{U}}$ and $\bar{\boldsymbol{V}}$ are two dense matrices of sizes $M \times R$ and $R \times N$, respectively; R being the effective rank of the matrix $\bar{\boldsymbol{A}}$. The two matrices $\bar{\boldsymbol{U}}$ and $\bar{\boldsymbol{V}}$ are constructed by the help of an iterative scheme, which can be seen as a rank-revealing LU decomposition [14], [17], which is stopped when the convergence is reached for a given tolerance threshold ϵ. It is very important to note that to compute $\bar{\boldsymbol{U}}$ and $\bar{\boldsymbol{V}}$, it is not necessary to calculate all the elements of the matrix $\bar{\boldsymbol{A}}$ to be compressed (unlike a singular value decomposition, SVD). Then, the resulting memory requirement is $(M + N)R$ instead of $M \times N$. For $M = N$, the compression is efficient if $2R \ll N$. In addition, the complexity of the matrix-vector product $\bar{\boldsymbol{A}}\mathbf{u} = \bar{\boldsymbol{U}}(\bar{\boldsymbol{V}}\mathbf{u})$ also requires $(M+N)R$ multiplications instead of MN. We define the compression ratio as

$$\tau = 1 - \frac{(M+N)R}{MN}. \tag{18}$$

If $R \ll (M, N)$, then τ is close to 1 (100% of compression), whereas if $\tau = 0$ (case for which $M = N = 2R$): the compression is not efficient. If $\tau < 0$ (e.g., $R = M$ or $R = N$), then ACA has a bigger storage requirement than that without ACA.

If the block matrices $\bar{\boldsymbol{Z}}_{i,i}$ can be stored, their calculations are done at the beginning and then the complexity with ACA becomes

$$C_{\mathrm{ACA}} = P\left[\mathcal{O}(N_0^3) + K_{\mathrm{SDIM}}\left(P-1\right)N_0^2\left(1-\bar{\tau}\right)\right] \tag{19}$$

where $\bar{\tau}$ is the mean compression ratio of the matrices $\{\bar{\boldsymbol{Z}}_{p,i}\}$ of compression ratio $\{\tau_{p,i}\}$ $(p \neq i)$ defined as

$$\bar{\tau} = \frac{1}{P(P-1)} \sum_{i=1}^{P} \sum_{p=1, p\neq i}^{P} \tau_{p,i}. \tag{20}$$

III. Numerical Results

The SDIM combined with ACA is tested on the electromagnetic scattering problem from random rough sea surfaces. Since the sea surface is highly conductive for microwave frequencies, the impedance (or Leontovich) boundary condition (IBC) is applied. To describe the sea surface height (its distribution is assumed to be a normal law), the Elfouhaily *et al.* [22] rough-

ness spectrum is applied. It depends on the wind speed, u_{10}, defined at ten meters above the sea mean level. In addition, the incident Thorsos [23] tapered wave is used to reduce the edges diffraction.

From the boundary integral equations, applying the MoM with point matching test functions and pulse basis functions, a linear system is obtained $\bar{\boldsymbol{Z}}\boldsymbol{X} = \boldsymbol{b}$, where $\bar{\boldsymbol{Z}}$ is the impedance matrix, $\boldsymbol{X}$ is the unknown vector of components the surface current ψ or $\partial\psi/\partial n$ sampled on the surface, and $\boldsymbol{b}$ is a known vector, related to the incident field sampled on the surface. The currents $\boldsymbol{X}$ is either computed from a direct LU inversion of $\bar{\boldsymbol{Z}}$ (for more details, see textbook [3], in which the MatLab codes are provided), or from SDIM or from SDIM combined with ACA. Then, from the Huygens principle, the scattered field is computed from radiating the currents ψ and $\partial\psi/\partial n$ and the normalized radar cross section (NRCS) is calculated.

A. Normalized Radar Cross Section

The simulation parameters are listed in Table I.

Fig. 1 plots the NRCS versus the scattering angles θ_s. The labels in the legends mean:

- "LU," the NRCS is computed using a direct LU inversion of the whole impedance matrix $\bar{\boldsymbol{Z}}$.
- "SDIM," the NRCS is computed using SDIM.
- "SDIM + ACA," the NRCS is computed using SDIM combined with ACA.

In addition, in the legend, the first number is the SDIM convergence order K_{SDIM} obtained when the relative residual error (RRE) is smaller than 0.01. The second number is the RRE value obtained for $k = K_{\mathrm{SDIM}}$ and defined as

$$\epsilon = \frac{\mathrm{norm}_{\theta_s}\left(\mathrm{NRCS}_{\mathrm{METHOD}} - \mathrm{NRCS}_{\mathrm{LU}}\right)}{\mathrm{norm}_{\theta_s}\left(\mathrm{NRCS}_{\mathrm{LU}}\right)}. \qquad (21)$$

SDIM converges if the spectral radius of the matrix $\bar{\boldsymbol{M}} = \bar{\boldsymbol{B}}\bar{\boldsymbol{V}}\bar{\boldsymbol{A}}^{-1}\bar{\boldsymbol{U}}$ is strictly smaller than one. For a matrix of large size, it is not possible to calculate the spectral radius because this operation is very time consuming. Thus, a means to know if SDIM converges, is to calculate the RRE on the surface currents or on the scattered field, and if the RRE increases with the order k, then SDIM fails because it does not converge.

Fig. 1 shows that the SDIM converges rapidly (at the order 1) and the value of the ACA convergence threshold is well chosen since the results closely match. For θ_i close to 90 degrees, a difference occurs between the NRCSs computed from LU and SDIM but the corresponding levels are very small (dB scale). For $K_{\mathrm{SDIM}} = 4$, this difference is insignificant. The compression ratios of the sub-domains coupling matrices $\tau_{p,i} \in [97.58; 99.44]\%$ (meanvalue $\bar{\tau} \approx 98.44\%$), which clearly shows that SDIM combined with ACA is very efficient. The number of blocks is 10 and the block sizes are 600×600.

Fig. 2 plots the current ratio $20\log_{10}(|\psi_{\mathrm{SDIM}}/\psi_{\mathrm{LU}}|) = 20\log_{10}|\psi_{\mathrm{SDIM}}| - 20\log_{10}|\psi_{\mathrm{LU}}| = \psi_{\mathrm{LU}}[\mathrm{dB}] - \psi_{\mathrm{SDIM}}[\mathrm{dB}]$ (difference in dB scale) versus the surface abscissa x for $x \in [-L/10; L/10]$, corresponding to 2 blocks. The vertical dashed-lines delimit the blocks and ψ_{LU} is the current computed from a direct LU inversion. The simulations parameters are listed in Table I. Recall that the order 0 of SDIM computes the current of each block by neglecting the coupling between the blocks. Then, at the edges of the blocks, the current value presents a discontinuity. Then, as K_{SDIM} increases, this effect decreases because the coupling between the block is better accounted for. Fig. 2 illustrates this phenomenon.

For the TE polarization (the results are not depicted), the conclusion is the same but SDIM converges more slowly. The convergence order is $K_{\mathrm{SDIM}} = 4$, instead of 1 for the TM polarization.

TABLE I
SIMULATION PARAMETERS OF FIG. 1. $\lambda_0 = 3 \times 10^8/f$ IS THE WAVELENGTH WHERE f IS THE FREQUENCY. THE BLOCKS HAVE THE SAME SIZES $N_0 \times N_0$.

Wind speed u_{10} [m/s]	5
Surface length L[m]	60
Number of samples N	6000
Frequency f [GHz]	3
Sampling step Δx [m]	$\lambda_0/10 = 0.1$
Incidence angle θ_i [°]	30
Thorsos wave parameter g [m]	$L/6 = 10$
Polarization	TM
Number of blocks P	10
ACA convergence threshold	0.001

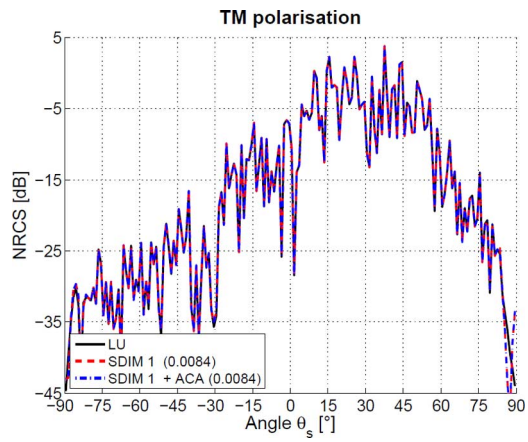

Fig. 1. NRCS versus the scattering angles θ_s for $f = 3$ GHz. The simulations parameters are listed in Table I.

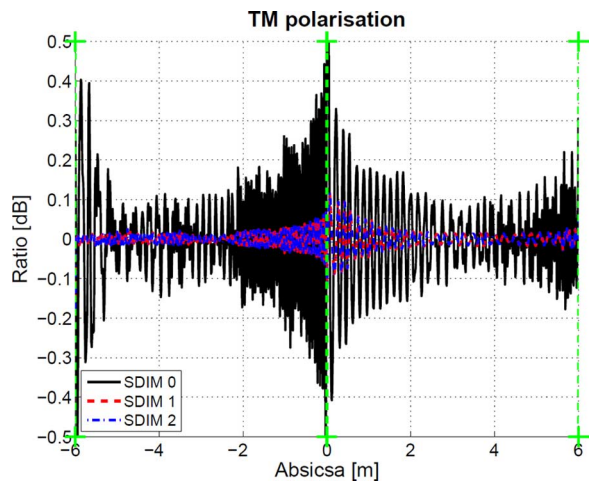

Fig. 2. Current ratio $|\psi_{\mathrm{SDIM}}/\psi_{\mathrm{LU}}|$ in dB (difference in dB scale) versus the surface abscissa x for $x \in [-L/10; L/10]$, corresponding to 2 blocks. The vertical dashed-lines delimit the blocks. The simulations's parameters are listed in Table I.

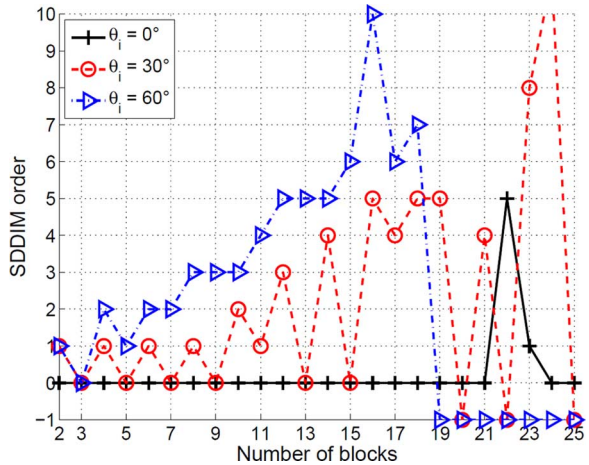

Fig. 3. Convergence order of SDIM K_{SDIM} versus the number of blocks P and the incidence angle θ_i. The simulation parameters are listed in Table II. In addition, $f = 3$ GHz, the polarization is TM, $u_{10} = 5$ m/s and $N = 10\,000$.

TABLE II
SIMULATION PARAMETERS OF FIGS. 3–7. $\lambda_0 = 3 \times 10^8/f$ IS THE WAVELENGTH WHERE f IS THE FREQUENCY.

Frequency f [GHz]	Changes
Incidence angle θ_i [°]	Changes
Polarization	Changes
Wind speed u_{10} [m/s]	Changes
Number of blocks P	Changes
Number of samples N	Changes
Surface length L[m]	$N\Delta x$
Sampling step Δx [m]	$\lambda_0/10 = 0.1$
Thorsos wave parameter g [m]	$L/6$
ACA convergence threshold	0.001
SDIM convergence threshold	0.01

B. Convergence Order and CPU Time

Fig. 3 plots the convergence order of SDIM K_{SDIM} versus the number of blocks P and the incidence angle θ_i. The simulation parameters are listed in Table II. In addition, the frequency f equals 3 GHz, the polarization is TM, the wind speed u_{10} equals 5 m/s and the number of unknowns N is 10 000. $K_{\mathrm{SDIM}} = -1$ means that SDIM has not converged. As we can see, SDIM converges rapidly and K_{SDIM} does not change significantly with P. As θ_i increases, K_{SDIM} increases and above $P = 18$ and for $\theta_i = 60°$, SDIM failed because it does not converge. Physically, as θ_i increases, the coupling between far sub-domains increases and then, the order K_{SDIM} increases.

Fig. 4 plots the CPU time versus the number of blocks P. The simulation parameters are the same as in Fig. 3 with $\theta_i = 30°$. The CPU time for LU is a constant number. As we can see for SDIM, the CPU time does not change with P because the convergence order K_{SDIM} is nearly independent of P and the CPU time is mainly allocated to the calculation of the elements of the impedance matrix $\bar{\boldsymbol{Z}}$ of constant sizes with respect to P. For SDIM + ACA, the CPU time is reduced in comparison to that obtained with SDIM and decreases when P increases because a) The mean compression ratio $\bar{\tau}$ ranges from 0.977 to 0.994 with a mean value of 0.985 (for $\theta_i = 30°$), accelerating the matrix-vector products in (12), b) The CPU time allocated to the calculation of the elements of the impedance matrices $\{\bar{\boldsymbol{Z}}_{i,i}\}$ ($i \in [1; P]$) decreases ($\mathcal{O}(N^2)/P$ with $N = 10\,000$).

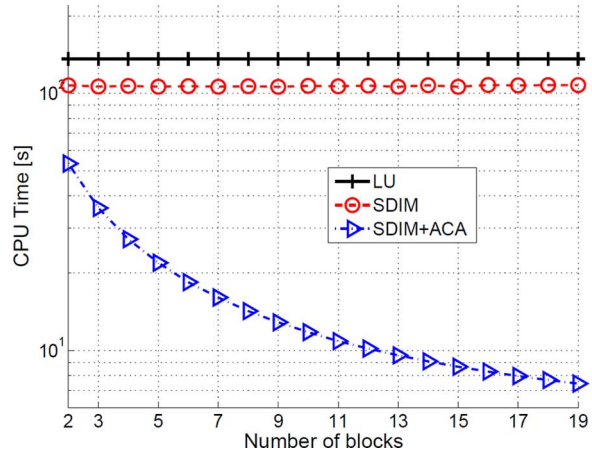

Fig. 4. CPU time versus the number of blocks P. The simulation parameters are the same as in Fig. 3 with $\theta_i = 30°$.

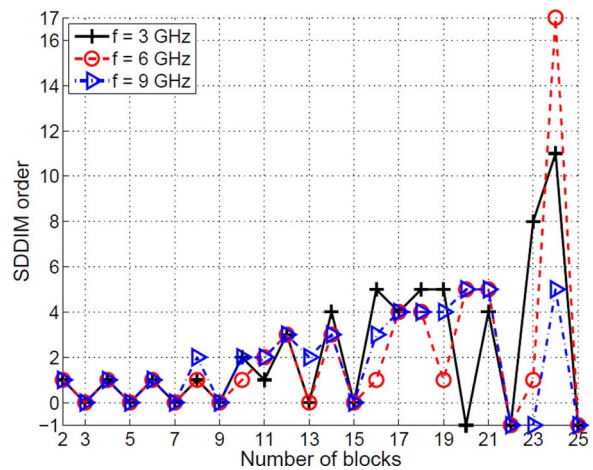

Fig. 5. Convergence order of SDIM K_{SDIM} versus the number of blocks P and the frequency. The simulation parameters are listed in Table II. In addition, $\theta_i = 30°$, the polarization is TM, $u_{10} = 5$ m/s and $N = 10\,000$.

Fig. 5 plots the convergence order of SDIM K_{SDIM} versus the number of blocks P and the frequency. The simulation parameters are listed in Table II. In addition, $\theta_i = 30°$, the polarization is TM, $u_{10} = 5$ m/s and $N = 10\,000$. As we can see, when the number of blocks is small, K_{SDIM} does not change with the frequency.

Fig. 6 plots the convergence order of SDIM K_{SDIM} versus the number of blocks P and the with speed u_{10}. The simulation parameters are listed in Table II. In addition, $f = 3$ GHz, $\theta_i = 30°$, the polarization is TM and $N = 10\,000$. As we can see, the sensitivities with respect to u_{10} are very weak until the number of blocks reaches 19 (at which time that the SDIM method is unstable).

Fig. 7 plots the convergence order of SDIM K_{SDIM} versus the number of blocks P and the polarization. The simulation parameters are listed in Table II. In addition, $f = 3$ GHz, $\theta_i = 30°$, $u_{10} = 5$ m/s, and $N = 10\,000$. As we can see, for the TE polarization, SDIM converges more slowly and as P increases, SDIM can fail for the TE and TM polarizations.

Fig. 8 plots the convergence order of SDIM K_{SDIM} versus the number of blocks P and for a given number of samples N. The simulation parameters are listed in Table II. In addition, $f = 3$ GHz, $\theta_i = 30°$ and $u_{10} = 5$ m/s. For the TE polarization

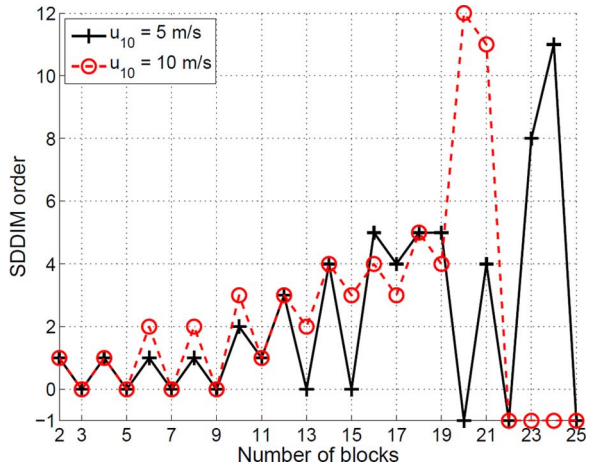

Fig. 6. Convergence order of SDIM K_{SDIM} versus the number of blocks P and the with speed u_{10}. The simulation parameters are listed in Table II. In addition, $f = 3$ GHz, $\theta_i = 30°$, the polarization is TM and $N = 10\,000$.

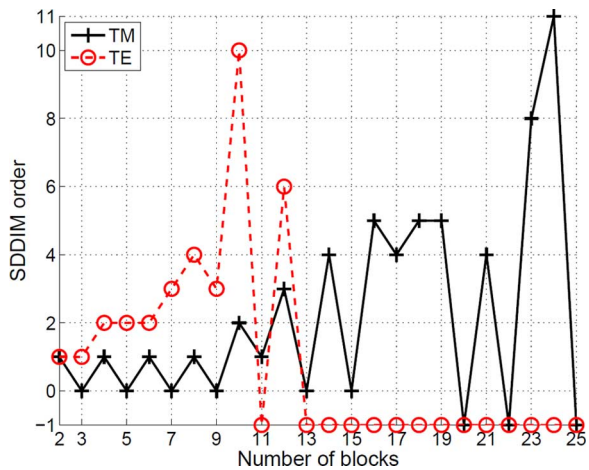

Fig. 7. Convergence order of SDIM K_{SDIM} versus the number of blocks P and the polarization. The simulation parameters are listed in Table II. In addition, $f = 3$ GHz, $\theta_i = 30°$, $u_{10} = 5$ m/s and $N = 10\,000$.

(top), as the surface length increases $L = 0.01\ N$ m and for a given P, the convergence order decreases because each subdomain length is larger and then, the coupling effect is already accounted for. As expected, as the number of blocks increases and for a given surface length, the convergence order increases. In addition, SDIM can fail if the number of blocks is too large. For the TM polarization, the proposed method is robust than in TE, because it converges with a smaller K_{SDIM} and with a larger P.

Fig. 9 plots the CPU time versus the number of unknowns N. The simulation parameters are listed in Table II. In addition, $f = 3$ GHz, $\theta_i = 30°$, $u_{10} = 5$ m/s, $P = \{2, 10\}$ and the polarization is TM. Fig. 10 plots the NRCS versus the scattering angles θ_s. The simulation parameters are the same as in Fig. 9 with $N = 25\,000$. As we can see in Fig. 9, the SDIM + ACA is very efficient in comparison to a direct LU inversion and as expected, as the number of blocs increases, the CPU time of SDIM + ACA decreases. For example, for $N = 25\,000$ and $P_2 = 10$, the CPU times is divided approximately by $P_2/P_1 = 10/2 = 5$ in comparison of that obtained for $P_1 = 2$. This is in agreement with (19). In Fig. 9, K_{SDIM} ranges from 0 to 2.

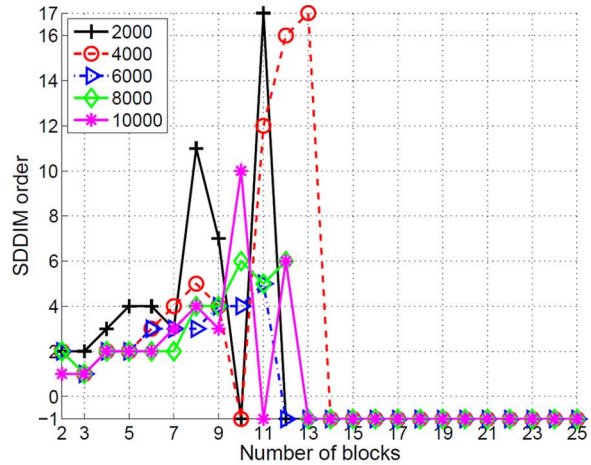

(a)

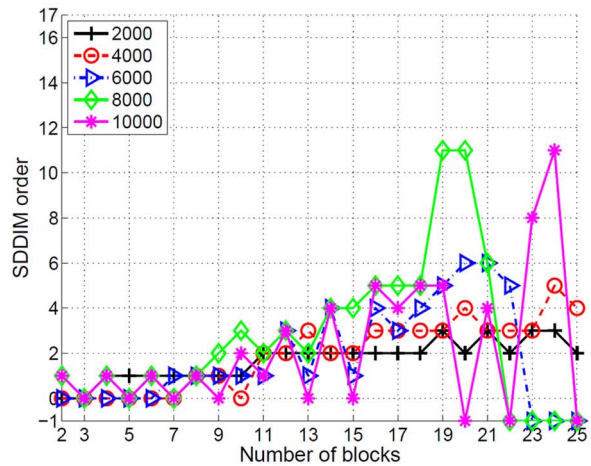

(b)

Fig. 8. Convergence order of SDIM K_{SDIM} versus the number of blocks P and for a given number of samples N. The simulation parameters are listed in Table II. In addition, $f = 3$ GHz, $\theta_i = 30°$, and $u_{10} = 5$ m/s. (a) TE polarization. (b) TM polarization.

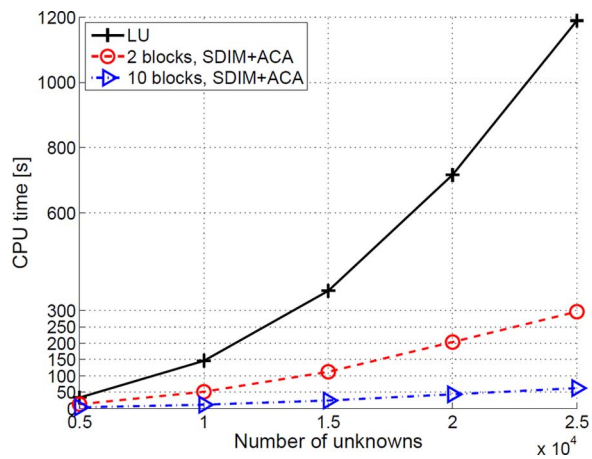

Fig. 9. CPU time versus the number of unknowns N. The simulation parameters are listed in Table II. In addition, $f = 3$ GHz, $\theta_i = 30°$, $u_{10} = 5$ m/s, $P = \{2, 10\}$ and the polarization is TM.

As in Fig. 1, Fig. 10 shows a good agreement between the methods, except for grazing scattering angles, for which the levels are very small.

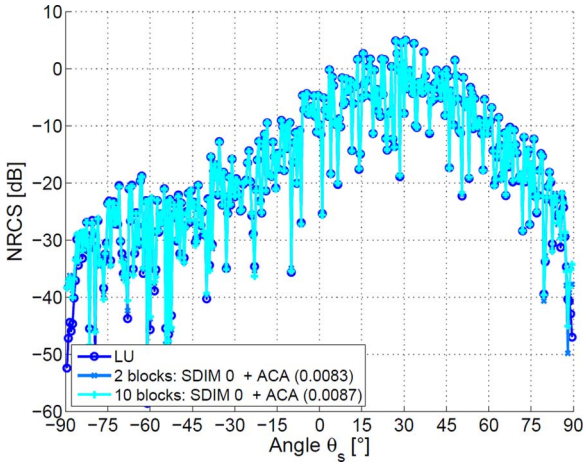

Fig. 10. NRCS versus the scattering angles θ_s. The simulation parameters are the same as in Fig. 9 with $N = 25\,000$.

C. Weak Coupling Approximation

Fig. 11 plots the NRCS versus the scattering angle θ_s and the ratio $\mathrm{NRCS_{SDIM}}/\mathrm{NRCS_{LU}}$ (difference in dB scale). In the legend, the first integer is the number of adjacent blocks P_0 taken in the sum over p of (12). This means in (12) that $p \in [i - P_0; i + P_0\}$ with $\max(p) = P$, $\min(p) = 1$ and $p \neq i$. As we can see, around the specular direction defined as $\theta_s = \theta_i$, the coupling between the sub-domains can be neglected and it becomes significant far from the specular direction, but the NRCS is small. In addition, the TE polarization is more sensitive to the coupling than the TM polarization, which explains why the convergence order of SDIM is larger for the TE polarization.

With this approximation of weak coupling between the sub-domains, for a given order k of SDIM, the number of matrix-vector products is

$$N_c = (2P_0 + 1)\left[P - 2\left(P_0 + 1\right)\right] - P + 2\sum_{n=1}^{P_0+1}\left(n + P_0\right)$$
$$= P_0\left(2P - P_0 - 1\right) \tag{22}$$

instead of $P(P-1)$, with $0 \leq P_0 < P$. From (19), the ACA complexity is

$$C_{\mathrm{ACA}} = P\left[\mathcal{O}(N_0^3) + K_{\mathrm{SDIM}}\left(P - 1\right)N_0^2\left(1 - \bar{\tau}\right)\eta_c\right] \tag{23}$$

where

$$\eta_c = \frac{N_c}{P(P-1)} \approx \frac{2P_0}{P} \text{ if } P_0 \ll P. \tag{24}$$

Then, the complexity is reduced by a factor $\eta_c \ll 1$ if $0 \leq P_0 \ll P$ for the calculation of the matrix-vector products and also for the memory requirement.

IV. Conclusion

In this paper, the new SDIM method computing the NRCS by a random rough highly conducting sea surface is presented. For the TM polarization, this method converges very rapidly, whereas for the TE, its convergence is slower and can fail when the sizes of the blocks, $\{N/P\}$ (P being the number of blocks), are too small in comparison to the number of samples N of the surface. For example, for $N = 10\,000$, SDIM can fail from $P \approx 20$. In addition, to accelerate the matrix-vector products for the coupling between the sub-domains, ACA is applied to reduce significantly the CPU time and the memory requirement. Indeed, the mean compression ratio is of the order of 98%, which makes SDIM+ACA very efficient. Applying the weak coupling approximation between the sub-domains, both the matrix-vector product and the memory requirement can be further reduced.

In the future, this method will be tested for the scattering of several perfectly conducting objects above a 1-D sea surface and for the scattering from a two-dimensional sea surface.

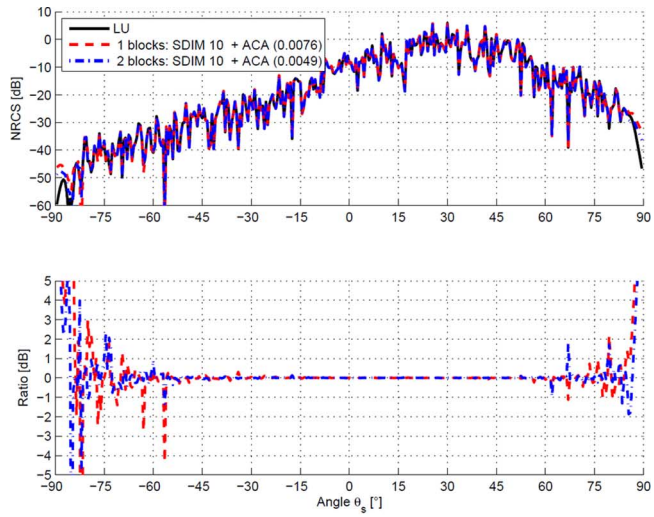

(a)

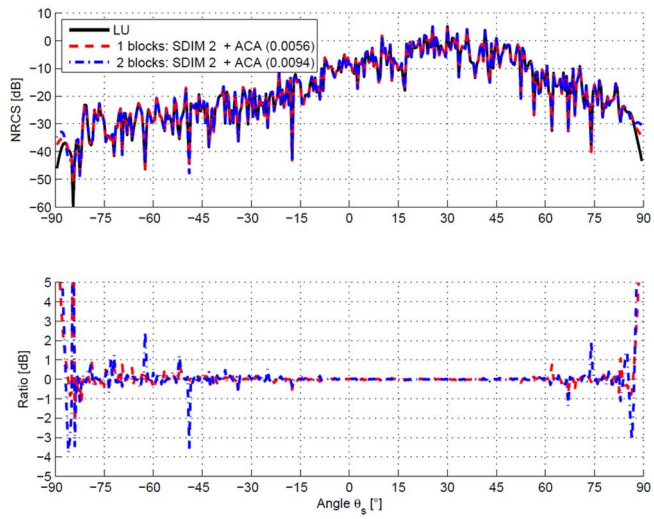

(b)

Fig. 11. First subplot: NRCS versus the scattering angle θ_s. Second subplot: NRCS ratio, $\mathrm{NRCS_{SDIM}}/\mathrm{NRCS_{LU}}$ (difference in dB scale) versus the scattering angle θ_s. The simulation parameters are listed in Table II. In addition, $f = 3$ GHz, $\theta_i = 30°$, $u_{10} = 5$ m/s, and $P = 10$, and $K_{\mathrm{SDIM}} = 2$ is computed from Fig. 7. (a) TE polarization: $K_{\mathrm{SDIM}} = 10$. (b) TM polarization:$K_{\mathrm{SDIM}} = 2$.

Acknowledgment

The authors would like to thank the anonymous reviewers for their useful comments.

REFERENCES

[1] R. F. Harrington, *Field computation by moment method*. New York: Macmillan, 1968.

[2] L. Tsang, J. A. Kong, K.-H Ding, and C. O. Ao, *Scattering of Electromagnetics Waves: Volume II. Numerical Simulations*. New York, NY, USA: Wiley Series on Remote Sensing, 2001.

[3] C. Bourlier, N. Pinel, and G. Kubické, *Method of Moments for 2D Scattering Problems. Basic Concepts and Applications*, FOCUS SERIES in WAVES , Ed. New York, NY, USA: Wiley-ISTE, 2013.

[4] D. Holliday, L. L. DeRaad, and G. J. St-Cyr, "Forward-backward: a new method for computing low-grazing angle scattering," *IEEE Trans. Antennas Propag.*, vol. 44, no. 5, pp. 722–729, May 1996.

[5] H. T. Chou and J. T. Johnson, "A novel acceleration algorithm for the computation of scattering from rough surfaces with the forward-backward method," *Radio Sci.*, vol. 33, pp. 1277–1287, 1998.

[6] M. R. Pino, R. Burkholder, and F. Obelleiro, "Spectral acceleration of the generalized forward-backward method," *IEEE Trans. Antennas Propag.*, vol. 50, no. 6, pp. 785–797, Jun. 2002.

[7] G. Kubické, C. Bourlier, and J. Saillard, "Scattering by an object above a randomly rough surface from a fast numerical method: extended PILE method combined with FB-SA," *Waves Random Complex Media*, vol. 18, pp. 495–519, 2008.

[8] G. Kubické and C. Bourlier, "A fast hybrid method for scattering from a large object with dihedral effects above a large rough surface," *IEEE Trans. Antennas Propag.*, vol. 59, no. 1, pp. 189–198, Jan. 2011.

[9] C. Bourlier, N. Pinel, and G. Kubické, "PILE method combined with PO for the scattering by coated cylinders, a rough layer and an object below a rough surface," *J. Opt. Soc. Amer. A*, vol. 30, no. 9, pp. 1727–1737, 2013.

[10] M. Kouali, G. Kubické, and C. Bourlier, "Electromagnetic Interactions Analysis between Two 3-D Scatterers Using the E-PILE Method Combined with the PO Approximation," *Progress in Electromag. Res. B*, vol. 58, pp. 123–138, 2014.

[11] V. V. S. Prakash and R. Mitra, "Characteristic basis function method: A new technique for efficient solution of method of moments matrix equations," *Microw. Opt. Technol.. Lett.*, vol. 26, no. 2, pp. 95–100, 2003.

[12] A. Yagbasan, C. A. Tunc, V. B. Ertürk, A. Altintas, and R. Mittra, "Characteristic basis function method for solving electromagnetic scattering problems over rough terrain profiles," *IEEE Trans. Antennas Propag.*, vol. 58, no. 5, pp. 1579–1589, May 2010.

[13] A. Heldring, J. M. Rius, J. M. Tamayo, J. Parrón, and E. Ubeda, "Multiscale compressed block decomposition for fast direct solution of method of moments linear system," *IEEE Trans. Antennas Propag.*, vol. 59, no. 2, pp. 526–536, Feb. 2011.

[14] M. Bebendorf, "Approximation of boundary element matrices," *Numer. Math.*, vol. 86, no. 4, pp. 565–589, 2000.

[15] M. Bebendorf and S. Rjasanow, "Adaptive low-rank approximation of collocation matrices," *Computing*, vol. 70, no. 1, pp. 1–24, 2003.

[16] S. Kurz, O. Rain, and S. Rjasanow, "The adaptive cross-approximation technique for the 3-D boundary element method," *IEEE Trans. Mag.*, vol. 38, no. 2, pp. 421–424, Mar. 2002.

[17] K. Zhao, M. N. Vouvakis, and J.-F. Lee, "The adaptive cross approximation algorithm for accelerated method of moments computations of EMC problems," *IEEE Trans. Electromag. Compat.*, vol. 47, no. 4, pp. 763–773, Nov. 2005.

[18] J. Shaeffer, "LU factorization and solve of low rank electrically large mom problems for monostatic scattering using the adaptive cross approximation for problem sizes to 1 025 101 unknowns on a PC workstation," in *Proc. IEEE Antennas Propag. Soc. Int. Symp.*, Sep. 9–15, 2007, pp. 1273–1276.

[19] J. Shaeffer, "Direct solve of electrically large integral equations for problem sizes to 1 M unknowns," *IEEE Trans. Antennas Propag.*, vol. 56, no. 8, pp. 2306–2313, 2008.

[20] J. M. Tamayo, A. Heldring, and J. M. Rius, "Multilevel adaptive cross approximation (MLACA)," *IEEE Trans. Antennas Propag.*, vol. 59, no. 12, pp. 4600–4608, Dec. 2011.

[21] A. Quarteroni, R. Sacco, and F. Sameri, *Méthodes Numériques: Algorithmes, Analyse et Applications*. New York, NY, USA: Springer-Verlag, 2007.

[22] T. Elfouhaily, B. Chapron, K. Katsaros, and D. Vandermark, "A unified directional spectrum for long and short wind-driven waves," *J. Geophys. Res.*, vol. 102, no. C7, pp. 15781–15796, 1997.

[23] E. I. Thorsos, "The validity of the Kirchhoff approximation for rough surface scattering using a Gaussian roughness spectrum," *J. Acoust. Soc. Amer.*, no. 83, pp. 78–92, 1988.

Christophe Bourlier was born in La Flèche, France, on July 6, 1971. He received the M.S. degree in electronics from the University of Rennes, Rennes, France, in 1995 and the Ph.D. degree from the SEI (SystèmeÉlectronique et Informatique) Laboratory, Nantes, France, in 1999.

He is now with IETR (Institute of Electronics and Telecommunications of Rennes, France) Laboratory, Nantes, at Polytech Nantes (University of Nantes, France). He is a Researcher at the National Center for Scientific Research working on electromagnetic wave scattering from rough surfaces (ocean like-surfaces) and objects for microwaves and infrared remote sensing applications and Radar signatures. He is author of more than 180 journal articles and conference papers.

Sami Bellez was born in Djerba, Tunisia, in 1981. He received the Ph.D. degree from the University of Paris VI, Paris, France, in 2010.

He has been with the L2S (Laboratory of Signal and System), Supélec, Gif-sur-Yvette, France, working in the field of electromagnetic scattering by forests. Then, he joined the L2E (Laboratory of Electronic and Electromagnetism) of the University of Paris VI for a work on bistatic synthetic aperture radar (SAR) imagery. Between 2011 and 2013, he was a Postdoctoral Research Fellow (financed by the French Space Agency CNES) with IETR (Institute of Electronics and Telecommunications of Rennes, France) Laboratory, Rennes. He is currently Research Scientist with the IETR, Nantes. His research interests include electromagnetic wave propagation and scattering in random media and from rough surfaces, microwave remote sensing, computational electromagnetics and SAR imaging techniques (interferometry and tomography).

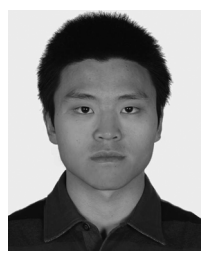

Hongkun Li was born in Guangdong, China, in July 1984. He received the B.S. and M.S. degrees in optics from the South China University of Technology, Guangzhou, China, in 2007 and 2010, respectively, and the M.S. degree and the Ph.D. degree in electronics from the University of Nantes, Nantes, France, in 2009 and 2012, respectively.

He is currently a Post-Doctoral Researcher with the IETR (Institute of Electronics and Telecommunications of Rennes, France) Laboratory at Polytech Nantes (University of Nantes, France). He works on infrared emission and reflection and microwave scattering problems concerning rough sea surfaces.

Gildas Kubické was born in Longjumeau, France, in September 1982. He received the Engineering degree and M.S. degree in electronics and electrical engineering from polytech Nantes, Nantes, France, in 2005 and the Ph.D. degree from the University of Nantes, Nantes, France, in 2008.

Then he was a Research Engineer at IREENA Laboratory (Institut de Recherche en Electrotechnique et Electronique de Nantes Atlantique), Nantes, France. In 2010, he joined the DGA (Direction Générale de l'Armement), French Ministry of Defense, where he works as an expert in the field of Radar signatures and electromagnetic stealth. He is in charge of the "Expertise in electroMagnetism and Computation" (EMC) Laboratory. His research interests include electromagnetic scattering and diffraction, radar cross section (RCS) measurement and modeling, asymptotic high-frequency methods, and fast numerical methods.